IEEE Access
Multidisciplinary | Rapid Review | Open Access Journal

Received 24 October 2022, accepted 8 November 2022, date of publication 14 November 2022, date of current version 18 November 2022.

Digital Object Identifier 10.1109/ACCESS.2022.3222082

RESEARCH ARTICLE

Extended Overmodulation Operation of Space Vector PWM for Traction Motor Control at Low Switching Frequency

GOKHAN ALTINTAS, (Member, IEEE), AND DERYA AHMET KOCABAS, (Member, IEEE)
Electrical Engineering Department, Istanbul Technical University, 34469 Istanbul, Turkey
Corresponding author: Gokhan Altintas (altintasgo@itu.edu.tr)

ABSTRACT There are several benefits of fully utilization of DC link voltage in railway traction applications in terms of increasing inverter output voltage, satisfying power-torque demand and component sizing. To meet traction system requirements; mostly space vector pulse width modulation (SVPWM) is preferred since it has lower harmonic contents and larger voltage reservoir than the others such as sinusoidal PWM (SPWM). Despite extended linear range of SVPWM, it may not be sufficient for traction systems due to high power requirements and low ratio of switching frequency to inverter output frequency. To overcome this problem, an algorithm having functional in the overmodulation range of SVPWM up to square wave modulation and applicable at low sampling, switching frequencies is proposed. Proposed method has ability of soft transition to overmodulation area and covers continuously all the section. Also, calculation of modulation signals is independent from sampling period. The detailed design method is given to calculate modulation signals to be compared with carrier wave in two different overmodulation sections and implemented. Implementations are used in practical experiments to verify the effectivity of proposed method. Moreover, practical experiments to ensure stability of the method are conducted with high powered traction motor in low switching frequency.

INDEX TERMS Closed loop systems, digital control, overmodulation, space vector pulse width modulation, traction motors.

I. INTRODUCTION

Power conversion from DC voltage to AC voltage is widely used in modern motor drive applications. Not only amplitude of voltage is variable, but also frequency alters in these applications to introduce variable speed operation. With the development of modern motor drives, voltage source pulse width modulation (PWM) inverters attracted more attention. These inverters employ capacitors in the DC-link to store temporary electrical energy. Switching elements such as IGBT, MOSFET are used to modulate DC voltage to obtain variable voltage and frequency waveform. Modulator primarily aims to generate the required switching signals for inverter switches. Output voltage value is determined by modulation ratio, which indicates the amount of DC link utilization. It varies with the duty cycle of switches and modulation method determines the maximum value of utilization. Sinusoidal PWM (SPWM), space vector PWM (SVPWM), selected harmonic elimination PWM (SHEPWM) methods are mostly used carrier based modulation algorithms in drive applications. SPWM has a basic structure that compares carrier wave with sinusoidal modulation signals, which makes this method easy to implement. SHEPWM requires solving complex mathematical equations to suppress relevant harmonic content and generation of lookup tables based on equation results. The results are predefined for each harmonic content to be inhibited and preloaded in controller unit such as DSP, FPGA and microcontroller. SVPWM necessitates complex online computations and has superior harmonic quality, minimized switching losses and wide range of operation. DC link utilization is commonly referred to the modulation ratio. In a three-phase voltage source inverter, modulation

The associate editor coordinating the review of this manuscript and approving it for publication was N. Prabaharan.

ratio is normalized to fundamental output voltage amplitude of the square wave operation. The maximum modulation ratio of SVPWM is 0.906, which is the upper limit of linear modulation.

Previous studies investigated nonlinear modulation range beginning from the upper limit of linear modulation [1]. Continuous control of inverters including overmodulation of SVPWM up to the six step mode was analyzed in a study that is one of the pioneers in the literature [1]. Discontinuous modulation method based on SVPWM was presented employing pulse dripping overmodulation sequence [2]. This method reduces the number of inverter switching while sustaining desired waveform quality with no regards to inverter current. However, the study accommodates complex calculations implementing the results for switching frequencies higher than 10 kHz.

Other studies involving SVPWM overmodulation show that the overmodulation range starting from 0.906 can be modeled as single mode up to square wave modulation which is 1 [3], [4], [5], [6], [7]. However, the analytical exploitations of these studies are complex and not easy to implement in digital control. In addition, [3], [4], [5] propose open loop modulation strategy, which is not adequate for the closed loop drive systems. The other paper comprising single section for overmodulation served high harmonic content and DC link voltage instability [6]. These are the natural results of the applied strategy related to the modification of both amplitude and angle of the reference voltage vector with inappropriate nonlinear gain values. In [7], a method to amplify the modulation waveform by a gain over the whole overmodulation section to apply compensated modulation technique. This method was shown to reduce the inverter gain and a feedforward controller must be included to guarantee a smooth transition in V/f control strategy for motor drives.

On the other hand, different SVPWM overmodulation strategies containing two different sub overmodulation zones were also introduced [8], [9], [10], [11], [12], [13], [14]. In [8], overmodulation range was divided into two different sections by using Fourier series expansion of reference voltage vector. It ignored the nonlinear relationship between modulation signal and inverter output voltage in the overmodulation zone, therefore gain was linearized by derived piecewise equations. Moreover, the implementation of the used algorithm incorporated complex analytical calculations and the practical study only consisted of V/f control. Extended results were obtained with a dual mode overmodulation strategy by simplifying the mathematical equations over extrapolation of undermodulation [9]. However, it was only valid for V/f control and was applicable only for high switching frequencies. Furthermore, no consideration for harmonic content minimization was provided. Authors used a synchronized SVPWM strategy related to superposition principle to derive the modulation signal as the sum of complex equivalent carrier-based modulated functions [10]. Although it was stated that the strategy is valid for low switching frequencies while serving a completely linear relationship between inverter output voltage and modulation index, no practical experiments were carried out and the success of the strategy was very susceptible to complex calculations. Other studies considered a modified current control for high-bandwidth current control to avoid current harmonics in vector controlled drives for overmodulation and six-step modes [11], [12]. The authors compensated the current harmonics that are injected according to the nature of PWM process and the current harmonics were created by exciting the motor windings with harmonic voltage component. These current harmonics were shown to be dominant in the overmodulation range and they were eliminated by introducing estimated current harmonics into the current controller. In [13], a modified version of existing overmodulation algorithms were presented. The study reduced the computational complexity in the overmodulation zone 2 while increasing the current harmonic distortion significantly in field oriented control of induction machine. In [14], authors analyzed field oriented rectangular control that adapts the predictive current control for overmodulation. However, the complexity of the controller was increased and the usage of flying capacitor inverters since modulation algorithm was restricted.

In [15], three-level voltage source inverters (VSI) were investigated and were simulated implementing both single mode and dual mode overmodulation strategies [15].

Minimum magnitude error and minimum phase error methods were implemented to a two-level VSI and complicated equations with double Fourier transform to reduce the harmonic distortions were presented [16]. Consequently, obtaining digital implementation of the methods becomes harder in practical experiments.

Recently in [17], an advanced synchronous SVPWM overmodulation method was proposed with a simplified hybrid mode PWM. This study merged SVPWM and six-step mode, and mathematical analytical equations of the method was given together with harmonic attributes. In [18], entire modulation range was divided into three modulation regions by using calculations based on the voltage space decomposition and superposition principles. The proposed method was applied to a dual three-phase PMSM drive and a smooth transition was obtained between linear modulation and overmodulation sections. In another study, the whole overmodulation area was separated into three local areas for a five-phase inverter by deriving linearized approximation with less computation while satisfying harmonic content were optimized [19]. It effectively controlled the voltage vectors causing the 3rd voltage harmonic existing in the output voltage of the five-phase inverter during overmodulation. However, it was only applied for resistive load and loss analysis was not carried out. Recent study which show the harmonic characteristics of synchronous SVPWM in full modulation range is carried [17]. Also, another studies implemented vector control for dual three phase PMSM and IPMSM in full modulation range [18], [20].

Railway tractions systems require low switching frequency related to the high power levels, while carrier based

modulation techniques suffer a lot as switching frequency decreases, hence the sampling frequency. This paper proposes an effective overmodulation strategy eligible up to square wave modulation which is still valid for low switching frequency applications such as railway traction control systems. Moreover, in the overmodulation region, the nonlinearity of the modulators and the inverter gain becomes dominantly effective on the stability of the output voltage. The controller can become non-functional relatedly and high precision in solving space vector equations is needed to avoid this non-functionality. In this paper, a new Modified Space Vector PWM (MSVPWM) method is described. An imaginary ''modified angle'' was introduced to the modulator to provide stability especially at the 2nd region, to support precision sensitivity, to obtain a decent voltage waveform at the output of the inverter, and to compensate any undesired effects. The newly calculated modified angle keeps the reference voltage vector inside the space vector hexagon, which provides stable operation of the controller. Moreover, the proposed method provides a smooth transition from linear modulation to overmodulation, thereby from overmodulation to square wave modulation. The sampling frequency of the proposed method was chosen two times of the switching frequency that helps in omitting the time-related terms in the modulation signal calculations which is another contribution of this study by reducing the calculation time. Furthermore, the proposed method was tested with a DSP controlled railway traction motor test set-up and it was shown that low switching frequency theoretical approaches and experimental results were in a very good harmony proving that the performance of proposed method is competent.

II. SPACE VECTOR MODULATION

Modulation is last stage of the control systems when switching is considered. In a power electronics circuit, desired power flow with less harmonic content is provided by adjusting the turn on and turn off times of the switching components and this approach is called as pulse width modulation (PWM). In a dedicated control system, there are several expectations from PWM strategy. These expectations can be described as to produce an inverter output voltage of which the fundamental component varies linearly with the control signal, and to provide a harmonic content away from the fundamental as far as possible which can be filtered by the motor windings. Therefore, the performance measures are utilization of DC link voltage and minimum harmful harmonic content. Utilization factor commonly refers to modulation index that depends on PWM methods used in inverters. In traction control applications, where there is limited DC link voltage and field weakening is used, it is very beneficial that the DC link voltage utilization factor of the PWM is high. In Figure 1, the basic scheme of a two-level three-phase inverter that supplies the traction motor is given.

Turning on-off times of six semiconductor switches provide energy flow from DC link to the traction motor. Highest DC link utilization factor is obtained by using square wave

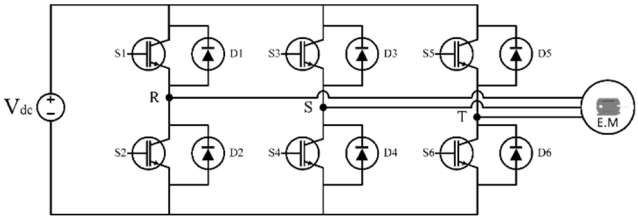

FIGURE 1. Two level three phase inverter supplying an e-motor.

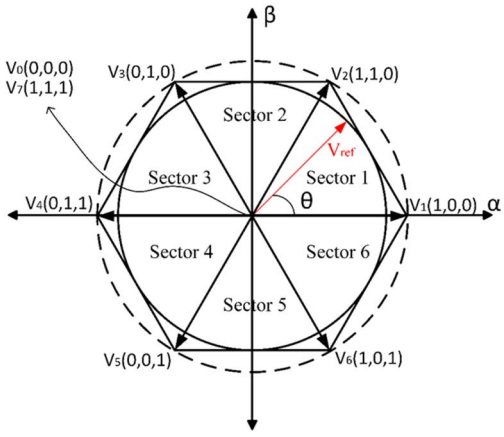

FIGURE 2. Space vectors representation on voltage space hexagon.

modulation which corresponds to six pulses among one cycle which causes nonlinearity at all. Modulation ratio of SVPWM is 0.906 and it can linearly sweep the hexagon of boundaries. In a two-level three-phase inverter, maximum output voltage amplitude with square wave modulation is $(2V_{dc})/\pi$ where the modulation ratio is 1, whereas maximum output voltage amplitude is $(V_{dc}/\sqrt{3})$ with SVPWM. The state of upper switches is represented in voltage vectors as 1 or 0 for turn-on and turn-off conditions, respectively. Modulation index boundary with voltage vectors on the space vector hexagon are shown in Figure 2. Zero space voltage vectors are located at the center of the hexagon which are V_0 and V_7.

In Figure 2, inverter output voltage V_{ref} which can be decomposed as V_α and V_β sweeps machine voltage space. To obtain V_{ref}, nearest space vectors (V_1 and V_2 in Figure 2) are utilized and are applied. The hexagon divided into six regions with 60 degrees to determine required sector information to determine which space vectors will be employed. Inscribed circle of the hexagon indicates the limits of V_{ref} that can be produced by using SVPWM. The region between hexagon and circumscribed circle (dashed circle) introduces overmodulation area.

Conventional space-vector modulation algorithm calculates switching intervals and then progress to the switching instants. t_1 and t_2 corresponds to the time to apply the adjacent voltage space vectors V_1, V_2, respectively, while t_0 implies the zero vector V_0 where all switches are on or off as in shown in Figure 3.

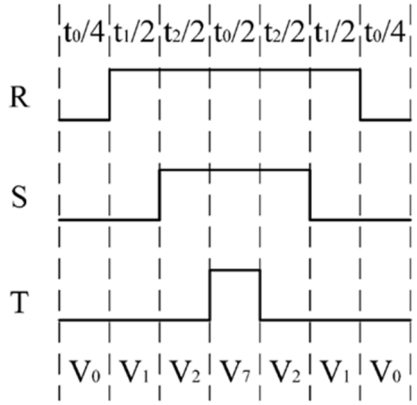

FIGURE 3. Switching signal waveforms employing adjacent and zero space vectors.

Relying on the symmetrical PWM model given in Figure 3, the times t_1, t_2 and t_0 are calculated by space vector modulation. The following set of example equations are written considering the voltage reference for a sector where α, T_s, V_{ref}, V_{dc} stand for sector angle, sampling time, voltage reference amplitude and DC link voltage, respectively.

$$t_1 = \frac{2\sqrt{3}T_s}{4V_{dc}} V_{ref} \sin({}^{\pi}/_{3} - \theta) \tag{1}$$

$$t_2 = \frac{2\sqrt{3}T_s}{4V_{dc}} V_{ref} \sin\theta \tag{2}$$

$$t_0 = \frac{T_s}{2} - (t_1 - t_2) \tag{3}$$

However, the voltage reference amplitude cannot provide sector information. Therefore, it requires a phase locked loop (PLL) algorithm to determine the sector it is in. Consequently, the complexity due to mathematical operations increases and it deviates from useful solution. Not only mathematical operations but also low sampling/switching frequency enhances complexity owing to high power traction application. Here, processing the α-β axis reference voltage amplitudes becomes the effective solution.

III. MODIFIED SPACE VECTOR MODULATION

In this section, a new Modified Space Vector PWM (MSVPWM) method is described. Conventional SVPWM is adequate at linear modulation zone, but is insufficient at over modulation zones. Here in this study, new modified reference voltage amplitude and angle values are described for overmodulation zones providing a better DC link utilization, a smooth transition between modulation zones and a decent voltage waveform at the output of the inverter. This method is applicable to low switching frequency applications like railway traction.

Figure 4-a and 4-b demonstrates the voltage vectors and reference voltage vector on space vector hexagon and involves the corresponding voltage waveforms representing linear modulation for conventional SVPWM. For simplicity,

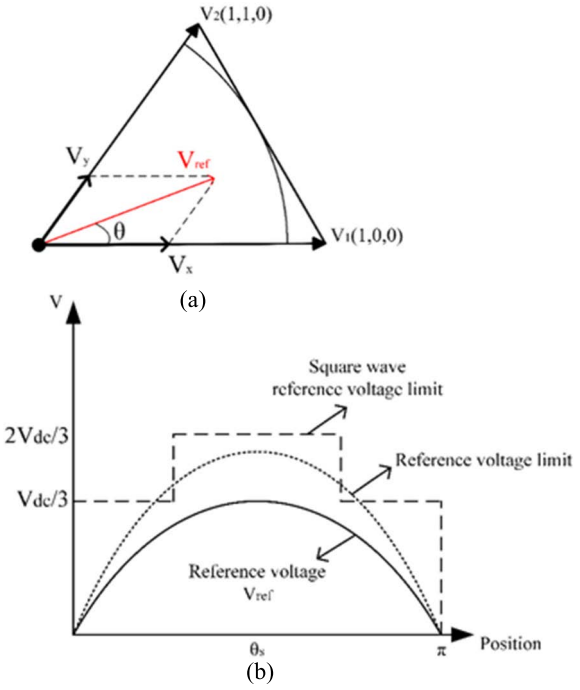

FIGURE 4. Representation of linear modulation via reference voltage vector, (a) position of reference voltage vector on hexagon, (b) voltage variation by change of position.

the representation of the hexagon is limited to the first sector only, and the waveform to π.

Figure 4-(a) shows the linear modulation range specifying modulation index lower than 0.907 for SVPWM and the reference voltage vector (V_{ref}) always stands in inscribed circle of hexagon and thus the corresponding waveform is given in Figure 4-(b).

Figure 5 demonstrates overmodulation zone 1 which is valid between 0.907 and 0.952. There are different methods for this zone as mentioned in Introduction section. Here in Figure 5, a chosen method by the authors is explained. The reference voltage vector tends to go beyond the hexagon as shown in Figure 5-(a) but it cannot surpass the side of the hexagon. Therefore, it is modified as given in Figure 5-(b). It has to track the dashed outer circle while it is inside of the hexagon, otherwise it pursues the hexagon side. Therefore, the actual reference voltage (V_{ref}) is needed to be modified to another value (V_{refm}) to satisfy this. The track route for V_{refm} is introduced with the red dashed line. Moreover, the corresponding voltage waveform becomes a composition of linear and sinusoidal segments as depicted in Figure 5 (c).

When the modulation index exceeds 0.9520 corresponding to overmodulation zone 2, the outer dashed circle is enlarged and at the end it comes across the circumscribed circle which crosses the corner of the hexagon given in Figure 6 (a). In order to obtain reference voltage amplitude, holding angle (θ_h) is introduced. As depicted in Figure 6-(b), reference voltage vector stops over space voltage vector (V_1) for the duration of the holding angle, θ_h. Then, it tracks side of

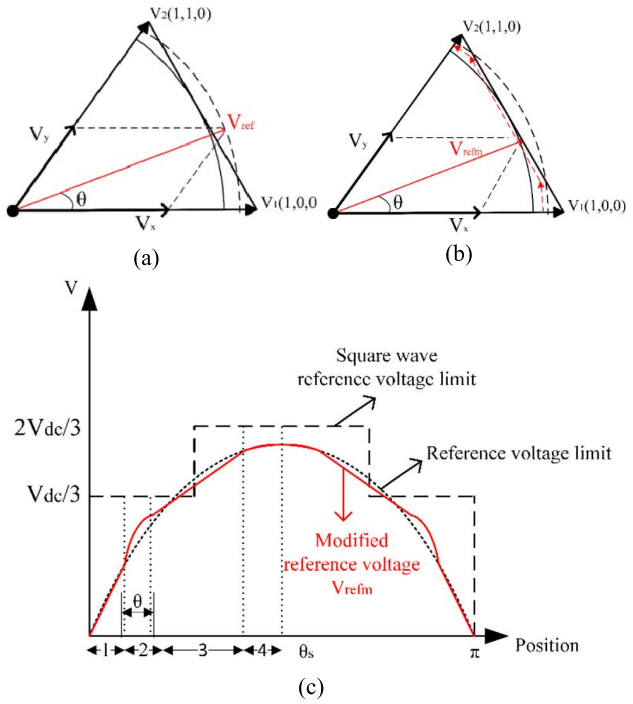

FIGURE 5. Representation of overmodulation zone 1 strategy, (a) position of reference voltage vector on hexagon, (b) modified position of reference voltage vector, (c) voltage variation by change of position.

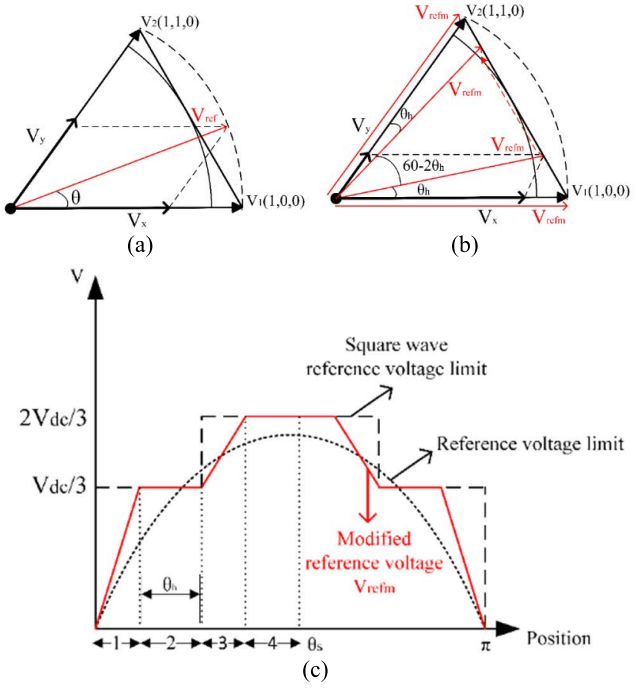

FIGURE 6. Representation of overmodulation zone 2 strategy, (a) position of reference voltage vector on hexagon, (b) modified position of reference voltage vector, (c) voltage variation by change of position.

the hexagon as it is shown with red dashed line. Finally, it jumps on space voltage vector (V_2) and stays there for the duration of holding angle. The output of the strategy yields

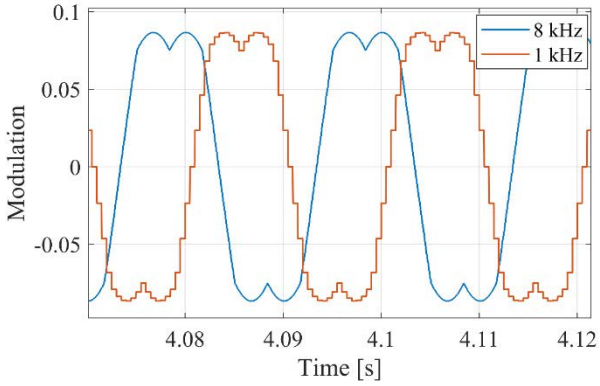

FIGURE 7. Effect of sampling frequency on modulation signal.

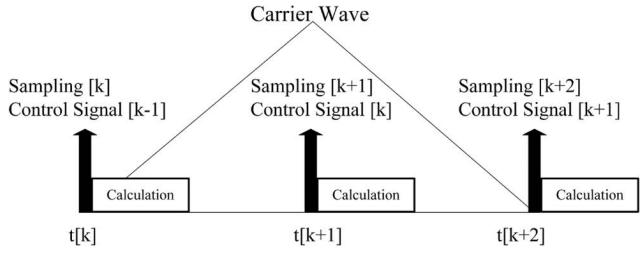

FIGURE 8. Measurements, calculations and outputs of PWM stages in DSP.

to the voltage waveform composed by the linear segments as illustrated in Figure 6-(c). When the modulation index reaches to unity, which comes across to square wave modulation, holding angle becomes 30° and it means that reference voltage vector only stands at space voltage vector positions. Under the circumstances of the both overmodulation zone 1 and zone 2, time duration of zero space voltage vectors, t_0, is suppressed.

A sector finding step is inserted to the algorithm which calculates the modulations signals. As the complexity of the mathematical expressions increase, the calculation time is extended and thus the effect of calculation delay becomes explicit. For a traction control application, where the switching/sampling frequency is around 1 kHz, the control algorithm deteriorates with this delay, hence it is necessary to exhibit fast and effective modulation strategy. Figure 7 represents the effect of sampling frequency on modulation signal. While the sampling frequency decreases, the attained waveform diverges from the desired one and reduces the performance of the digital control system.

Furthermore, in order not to amplify the switching noises, analog signals are measured before the digital signal processor (DSP) generates PWM signals in the closed loop control system. Analog digital conversion (ADC) measurements, control system calculations and PWM outputs are shown in Figure 8. Sampling frequency is chosen two times of the switching frequency to eliminate undesired effects in motor control applications.

TABLE 1. Equations for voltage reference vector in overmodulation zone 1.

$V_{e1} = m_1\theta_s$	$m_1 = 2v_{dc}/\pi$	$0 < \theta_s < -\theta$
$V_{e2} = V^*_{refm}\ \sin\theta_s$	$V^*_{refm} = \frac{2\,V_{dc}(\pi/6-\theta)}{\pi\sin(\pi/6-\theta)}$	$\pi/6-\theta < \theta_s < \pi/6+\theta$
$V_{e3} = A + (m_1/2)\,\theta_s$	$A = v_{dc}/6$	$\pi/6+\theta < \theta_s < \pi/2-\theta$
$V_{e4} = V^*_{refm}\ \sin\theta_s$	$V^*_{refm} = \frac{2\,V_{dc}(\pi/6-\theta)}{\pi\sin(\pi/6-\theta)}$	$\pi/2-\theta < \theta_s < \pi/2$

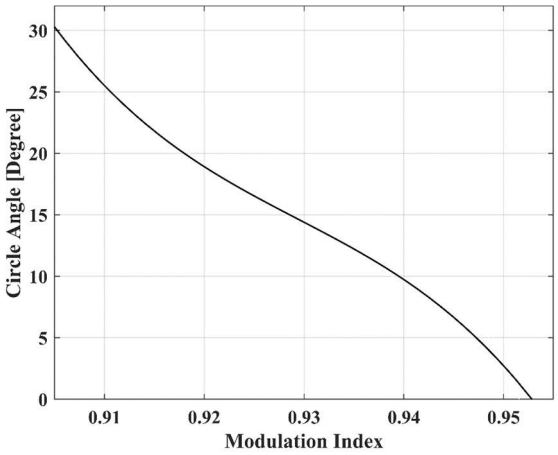

FIGURE 9. Circle angle variation by modulation index.

According to the above approaches, an algorithm based on DSP is developed which is effective between 0 and 1 modulation index ranges and is independent from switching frequency (f_s) as it is shown in the next part of this manuscript.

Considering field oriented control strategy, d-q voltage references (V_d, V_q) which are the output of current controllers are transformed into α-β voltages (V_α, V_β) by using Inverse Park transformation. Then, the switching instants (not switching intervals t_1, t_2, t_0) for three phases (t_{RON}, t_{SON}, t_{TON}) are calculated directly with simple sector finding algorithm. In the overmodulation area, ''imaginary modified reference voltage vector (V_{refm})'' is introduced having its own new modified amplitude and angle inside the hexagon. The mathematical equations representing V_{refm} are derived for each overmodulation sections and then expressions are solved to extract an amplifier coefficient changing with variation of modulation index.

Based on Figure 5-(c), V_{refm} in overmodulation section 1 can be composed by following equations as given in Table 1.

When the above equations solved by iteratively, θ is obtained as a function of the modulation index as shown in Figure 9 and it is named as circle angle since the reference voltage vector tracks the circle for the time duration θ demonstrated in Figure 5 (b).

In a similar way, based on Figure 6-(c), V_{refm} in overmodulation section 2 is determined by following equations as given in Table 2. However, it is designated to modify not only the amplitude of the reference voltage vector but also its angle. θ_m is the modified angle of the modified reference voltage vector (V_{refm}) while θ_s corresponds to any angle on a sector of the voltage space. θ_m mainly contributes to compensation of voltage waveform deterioration due to θ_h and its key point of the approach.

When the modified reference voltage calculated by the equations above match with the reference voltage, the

TABLE 2. Equations for voltage reference vector in overmodulation zone 2.

$$\theta_m = \begin{cases} 0 & 0 < \theta_s < \theta_h \\ \frac{\theta_s - \theta_h}{\pi/6-\theta_h}\frac{\pi}{6} & \theta_h < \theta_s < \pi/3-\theta_h \\ \pi/3 & \pi/3-\theta_h < \theta_s < \pi/3 \end{cases}$$

$V_{e1} = m_1{}'\theta_s$	$m_1{}' = \frac{V_{dc}}{3(\pi/6-\theta_h)}$	$0 < \theta_s < \pi/6-\theta_h$
$V_{e2} = V_{dc}/3$		$\pi/6-\theta_h < \theta_s < \pi/6+\theta_h$
$V_{e3} = A' + m_2\,\theta_s$	$A' = \frac{V_{dc}(\pi/6-3\theta_h)}{3(\pi/3-2\theta_h)}$ $m_2{}' = \frac{V_{dc}}{3(\pi/3-2\theta_h)}$	$\pi/6+\theta_h < \theta_s < \pi/2-\theta_h$
$V_{e4} = 2V_{dc}/3$		$\pi/2-\theta_h < \theta_s < \pi/2$

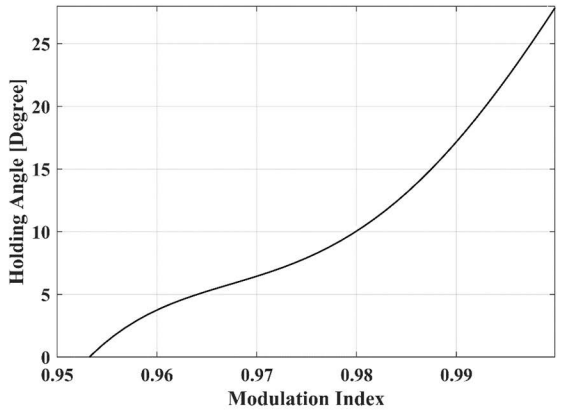

FIGURE 10. Holding angle variation by modulation index.

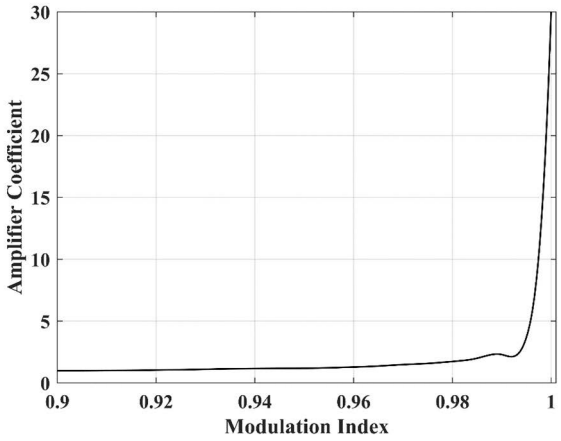

FIGURE 11. Amplifier coefficient variation by modulation index.

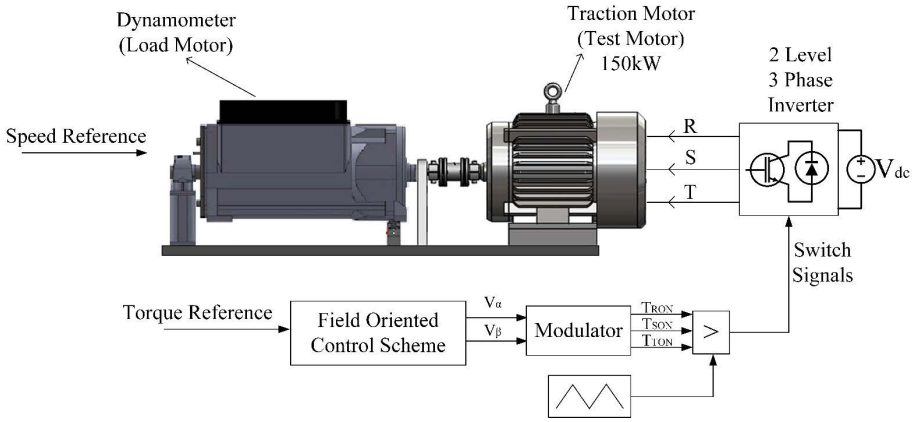

FIGURE 12. Principal control and test bench.

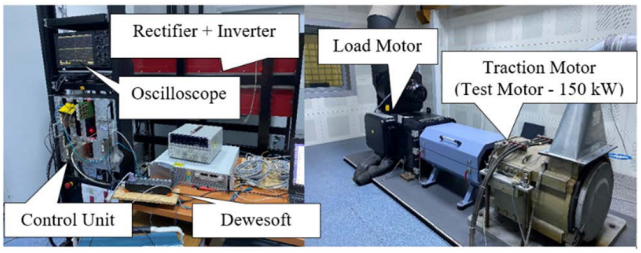

FIGURE 13. Practical test bench.

equations are solved iteratively by using the modulation index variation and then, θ_h is procured for each modulation index value as shown in Figure 10.

When the modulation signal reaches a peak value of 1 while the modulation index converges to 1 and then, the space vector modulation signals shown in Figure 7 becomes a square wave modulation signal converging the turn-on interval to 30°. Briefly, an amplified modulation signal is calculated in both overmodulation zones with the given equations by considering θ_m for overmodulation zone 2. This signal is then divided with base space vector modulation signal to obtain an amplifier coefficient. The change of this variation coefficient according to modulation index is given in Figure 11. As can be seen from Figure 11, amplifier coefficient goes to infinity while the modulation index converges to 1.

All approaches, assumptions and proposals are extended for other sectors of the space vector hexagon and then concluded by the given equations where g_R, g_S, g_T are the pre-modified modulation signals for the related phase. As can be seen from the sector equations, all equations are independent from sampling frequency as follows:

Sector 1 ($0< \theta <60$) and Sector 4 ($180< \theta <240$);

$$g_R = \frac{3}{2V_{dc}} x(-U_\alpha - \frac{U_\beta}{\sqrt{3}}) \tag{4}$$

$$g_S = \frac{3}{2V_{dc}} x(U_\alpha - \sqrt{3}U_\beta) \tag{5}$$

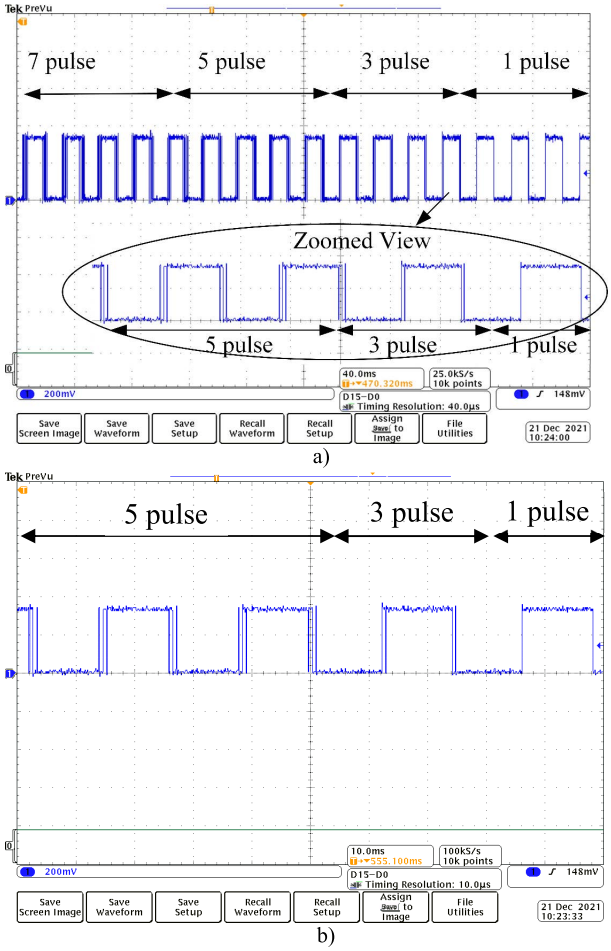

FIGURE 14. Switching pulses for different modulation indexes, a) Pulse trains variation with modulation index increases b) Extended view to pulse transition instants.

$$g_T = \frac{3}{2V_{dc}} x(U_\alpha + \frac{U_\beta}{\sqrt{3}}) \tag{6}$$

Sector 2 ($60 < \theta < 120$) and Sector 5 ($240 < \theta < 300$);

$$g_R = \frac{3}{2V_{dc}} x(-2U_\alpha) \tag{7}$$

$$g_S = \frac{3}{2V_{dc}} x(-\frac{2U_\beta}{\sqrt{3}}) \quad (8)$$

$$g_T = \frac{3}{2V_{dc}} x(\frac{2U_\beta}{\sqrt{3}}) \quad (9)$$

Sector 3 ($120 < \theta < 180$) and Sector 6 ($300 < \theta < 360$);

$$g_R = \frac{3}{2V_{dc}} x(-U_\alpha + \frac{U_\beta}{\sqrt{3}}) \quad (10)$$

$$g_S = \frac{3}{2V_{dc}} x(U_\alpha - \frac{U_\beta}{\sqrt{3}}) \quad (11)$$

$$g_T = \frac{3}{2V_{dc}} x(U_\alpha + \sqrt{3}U_\beta) \quad (12)$$

Switching instants to be compared with carrier wave are obtained as follows; (c is the amplifier coefficient in the overmodulation sections as depicted in Figure 9, otherwise it equals unity.)

$$T_{RON} = \frac{(1 + cg_R)}{2} \quad (13)$$

$$T_{SON} = \frac{(1 + cg_S)}{2} \quad (14)$$

$$T_{TON} = \frac{(1 + cg_T)}{2} \quad (15)$$

In the algorithm, numerators of the T_{RON}, T_{SON}, T_{TON} are limited to 0 at the lower boundary and to 2 at the upper boundary. Therefore, these signals stay in the range of 0-1 so that they can be compared with a carrier comparator wave created by the PWM module of DSP. The determined sector defines the position (θ) of the α-β voltage references on space vector hexagon and it is equal to the arctangent of V_α/V_β.

IV. EXPERIMENTAL RESULTS

Firstly, algorithm was validated on simulations then the routine was implemented on a Texas Instruments TMS320F28335 DSP. Principal control and test bench was implied as in Figure 12 while actual practical test setup is shown in Figure 13. Field oriented control scheme is composed of current controller with feed-forward and active damping resistance, torque controller, field controller and back EMF based observer. Modulator refers to proposed algorithm given in the previous section.

The modulation algorithm runs satisfactorily in undermodulation and overmodulation sections and at square wave mode without any additional structural changes. While modulation index is increased, the number of pulses of switch signals are reduced. They approach to 1 pulse at the square wave mode, whereas 3-5-7 or more pulses in overmodulation and undermodulation range. Switch signals during transition from undermodulation to overmodulation were shown in Figure 14 in aspect of pulse trains with pulse transition instants in zoomed view manner.

All related measured data were observed with oscilloscope and were acquired with Dewesoft which is CAN data acquisition device. The modulation signals were calculated in DSP of traction control unit. The traction motor used in tests is a squirrel cage induction motor with a rated power of 150 kW.

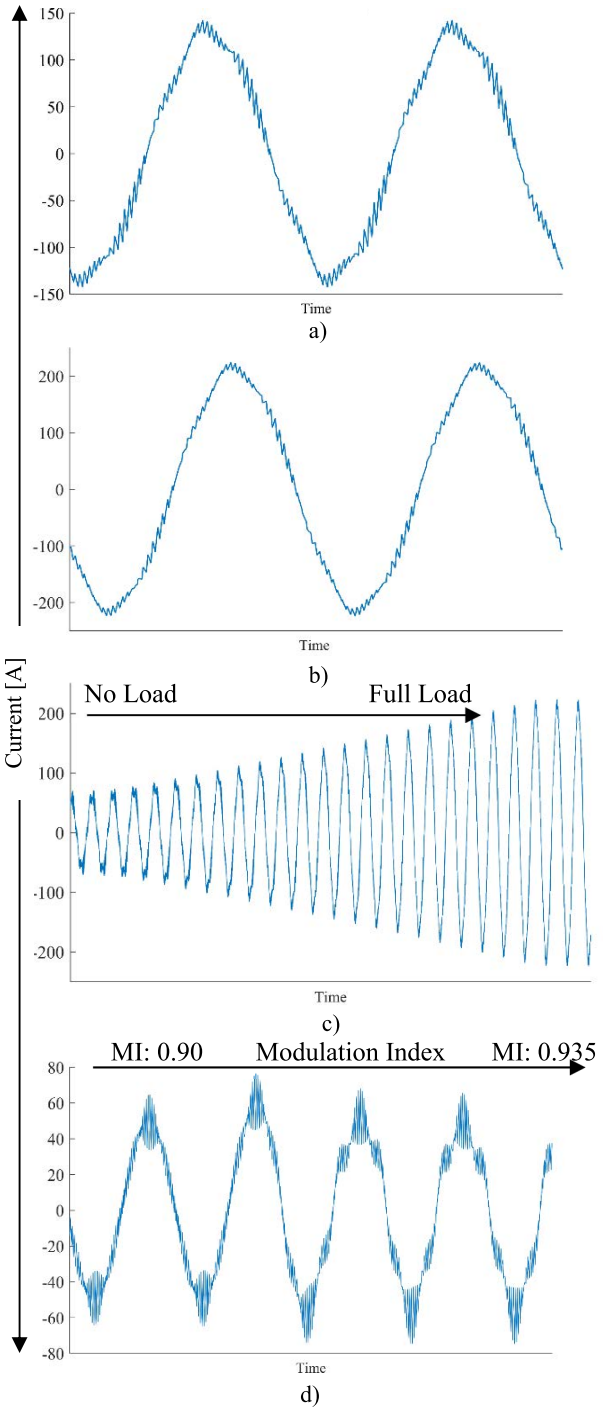

FIGURE 15. Overmodulation range 1 experimental results, a) Half load steady-state phase current of motor b) Full load steady-state phase current c) Dynamic behavior of phase current while loading with full load d) Transition from undermodulation to overmodulation.

The switching frequency is 1000 Hz and the motor was accelerated to 200 rpm at 850 V DC link. Current vs time representing both half load and full load conditions, dynamic change of phase current at no-load & full load transition and linear & overmodulation transition for overmodulation zone 1, overmodulation zone 2 and square wave mode are

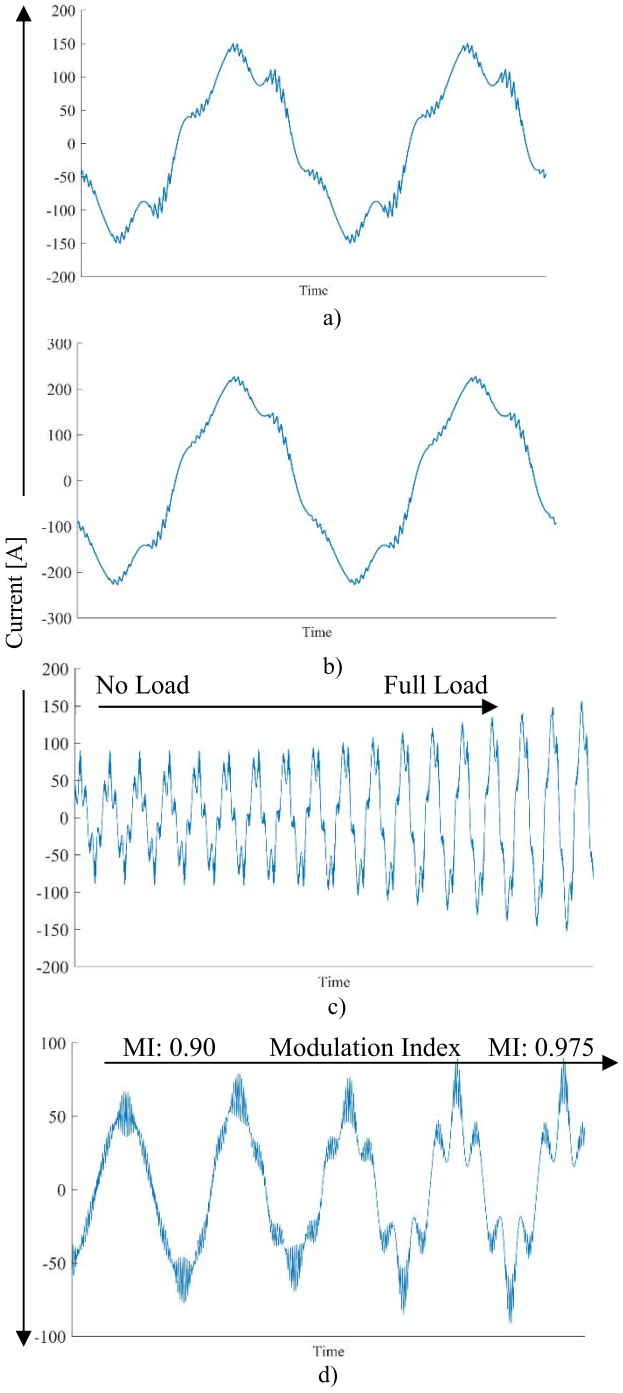

FIGURE 16. Overmodulation range 2 experimental results, a) Half load steady-state phase current of motor b) Full load steady-state phase current c) Dynamic behavior of phase current while loading with full load d) Transition from undermodulation to overmodulation.

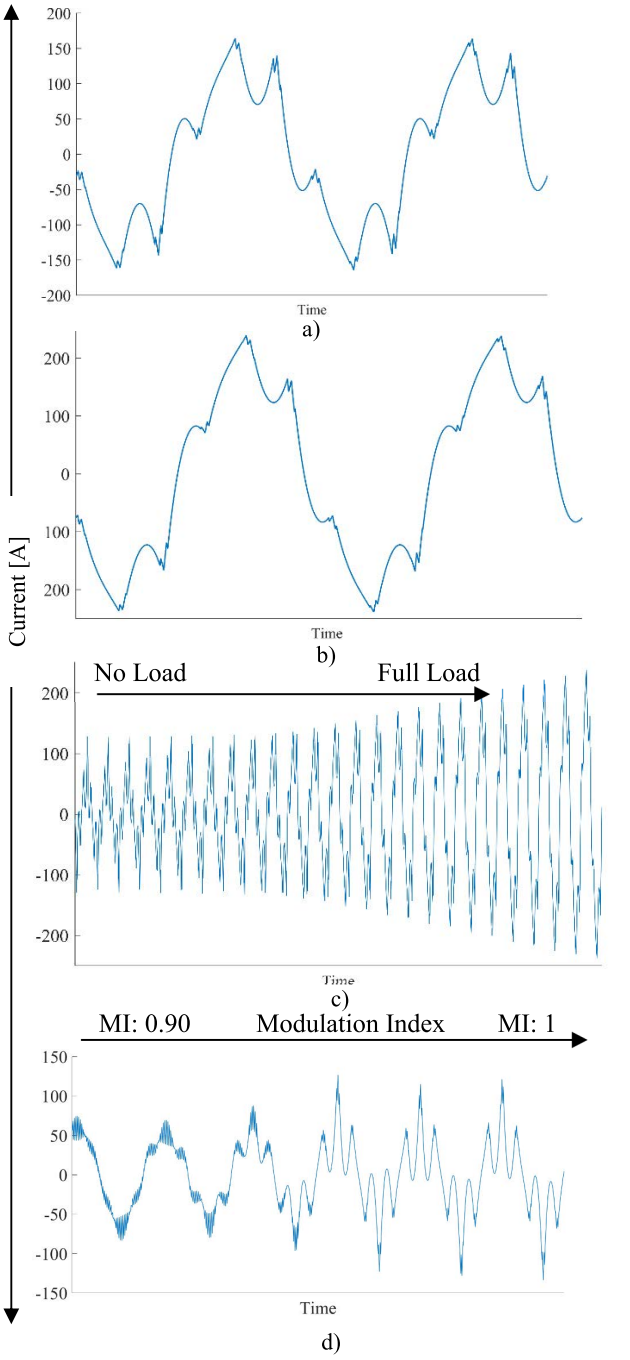

FIGURE 17. Square wave (six step) mode experimental results, a) Half load steady-state phase current of motor b) Full load steady-state phase current of motor c) Dynamic behavior of phase current while loading with full load d) Transition from undermodulation to overmodulation.

given in Figure 15, Figure 16 and Figure 17, respectively. Reference voltage values can be described as ($2V^*_{dc}MI/\pi$) and it changes for each MI point in the demonstrations given in Figure 15, Figure 16 and Figure 17. Angle information is also defined for each MI point with help of Figure 9 and Figure 10. Exact phase angle information is indicated that the reference voltage scans the whole 360-degree space voltage plane so it completes one turn with one modulation signal frequency. Standstill position of rotor states the 0-degree angle.

As it can be seen from Figure 15, 16 and 17, the experimental results satisfy the requirements and validate the approach. Section (a) of each figure shows the steady-state phase current of the traction motor in the condition of half load while

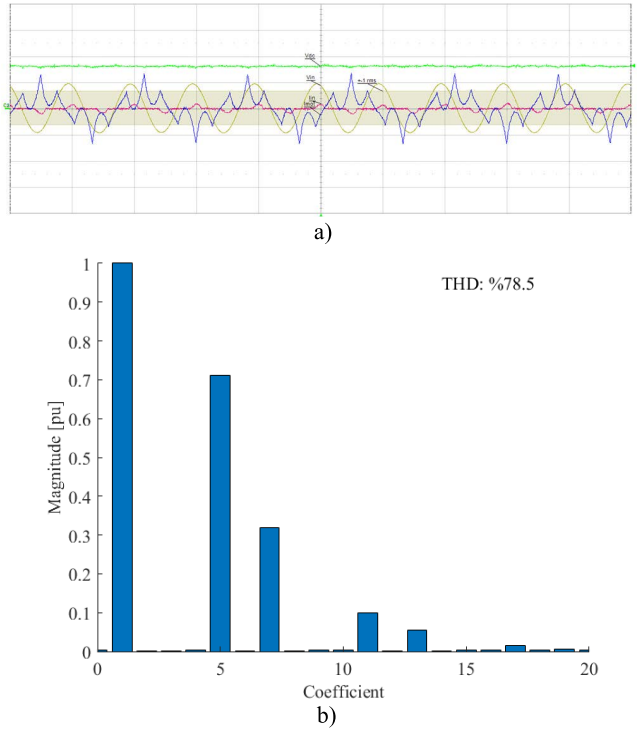

FIGURE 18. a) Used phase current (blue) instant in no load square wave mode condition b) THD value and Fourier spectrum of represented phase current in a).

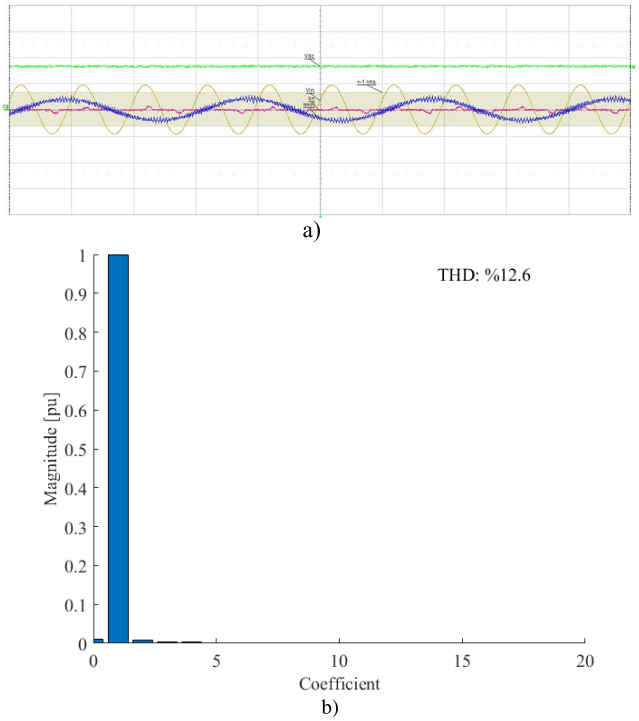

FIGURE 19. a) Used phase current (blue) instant in full load overmodulation range 1 b) THD value and Fourier spectrum of represented phase current in a).

section of (b) show full load condition. Moreover, sections of (a) and (b) is a follow up of sections (c) and (d). Because, section (d) shows the transition instant and it gets loaded like in (c) and then section (a) or (b) is occurred. Transition from undermodulation to any point of overmodulation range takes place smoothly and no current spikes were observed. Phase current waveforms diverge from sinusoidal waveform as modulation index increases. However, current waveforms become more sinusoidal as the load ratio increases, as it is expected.

To make a quantitative analysis, total harmonic distortion (THD) as performance index is derived in two different conditions. First condition is no load condition in square wave mode which means obviously worst condition in aspect of THD as shown in Figure 18 as well as Fourier spectrum with the processed instant of phase current for THD. Figure 18 (a) represents similar manner with Figure 17 (d). Second condition is full load in overmodulation range 1 as implied in Figure 19 with Fourier spectrum and also it contains the phase current plot which is processed for THD.

Simulations studies were not included in order not to overwhelm the paper. But it is certain that simulation results better due to nonlinearities, parasitic effects, measurement errors and so on.

THD value of %12.6 symbolizes the closest operation to linear PWM range while THD value of %78.5 demonstrates most far operation point. Therefore, it is obvious that THD performance indexes of proposed overmodulation algorithm

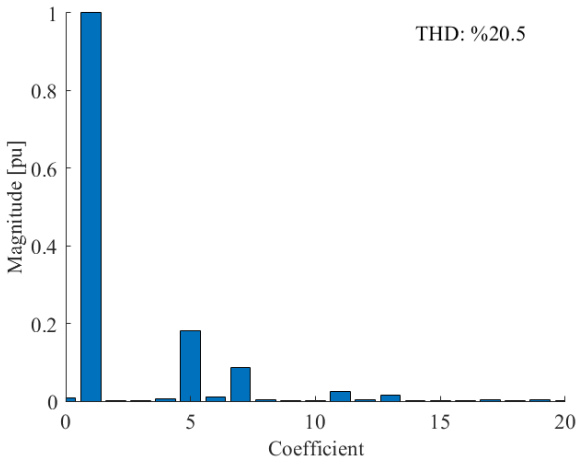

FIGURE 20. THD and Fourier spectrum of full load condition in square wave mode.

vary between %12.6 and %78.5. Figure 20 is given to show THD and Fourier spectrum of full load condition in square wave mode. THD values are reasonable because low switching frequency generates harmonic contents and distorts the current waveform. If switching frequency is increased the THD values will be descended.

Proposed method is compared with [17] in aspect of THD and it is found that harmonic contents in the six step operation are higher than the compared work. In other circumstances THD values seem lower. It should be noted that compared

work uses synchronous PWM method which runs with variable switching scheme.

V. CONCLUSION

This paper presents the detailed step by step design approach and implementation of a novel modulation algorithm which is valid up to square wave modulation for a low switching frequency application. Problems and requirements were discussed and then solutions were addressed with detailed descriptions supported by clear demonstrations. The proposed algorithm is independent of sampling frequency and is applicable to all motor control systems which use peak and zero point of triangular carrier waveform for sampling instant. Moreover, the given approach outputs the switching turn on-off time instead of on-off duration and thus, they can be linked with compare registers of PWM module of DSP. Introduced angle modification term which is valid in overmodulation section 2 amplifies the modulation signal slightly to eliminate the undesired effects of low switching/sampling frequency during calculation. Unlike similar studies running synchronous PWM method, it is not needed to change switching frequency so it is adequate for constant switching frequency applications. Experimental results show that modulation algorithm is competent at any point of undermodulation and overmodulation range and smooth during transition from undermodulation to overmodulation. The algorithm also involves a state of sustainable and stable while loading condition varies. As a future work, proposed algorithm will be tested in higher switching frequencies.

REFERENCES

[1] J. Holtz, W. Lotzkat, and A. M. Khambadkone, "On continuous control of PWM inverters in the overmodulation range including the six-step mode," *IEEE Trans. Power Electron.*, vol. 8, no. 4, pp. 546–553, Oct. 1993, doi: 10.1109/63.261026.

[2] H.-J. Park and M.-J. Youn, "A new time-domain discontinuous space-vector PWM technique in overmodulation region," *IEEE Trans. Ind. Electron.*, vol. 50, no. 2, pp. 349–355, Apr. 2003, doi: 10.1109/TIE.2003.809402.

[3] S. Bolognani and M. Zigliotto, "Novel digital continuous control of SVM inverters in the overmodulation range," *IEEE Trans. Ind. Appl.*, vol. 33, no. 2, pp. 525–530, Mar. 1997, doi: 10.1109/28.568019.

[4] L. W. J. Zhang Liu, X. H. Wen, and G. L. Chen, "A novel algorithm of SVPWM inverter in the overmodulation region based on fundamental voltage amplitude linear output control," *Proc.-Chin. Soc. Elect. Eng.*, vol. 25, no. 19, pp. 12–18, 2005.

[5] L. Zhang, "A novel strategy of SVPWM over modulation for piecewise continuous control," *J. Electr. Mach. Control*, vol. 32, no. 7, pp. 19–23, 2005.

[6] Z. Xu, D. Liu, X. Zhao, and J. Ren, "Over-modulation control strategy of SVPWM review," in *Proc. Chin. Control Decis. Conf. (CCDC)*, May 2016, pp. 3192–3196, doi: 10.1109/CCDC.2016.7531532.

[7] R. J. Kerkman, D. Leggate, B. J. Seibel, and T. M. Rowan, "Operation of PWM voltage source-inverters in the overmodulation region," *IEEE Trans. Ind. Electron.*, vol. 43, no. 1, pp. 132–141, Feb. 1996, doi: 10.1109/41.481418.

[8] D.-C. Lee and G.-M. Lee, "A novel overmodulation technique for space-vector PWM inverters," *IEEE Trans. Power Electron.*, vol. 13, no. 6, pp. 1144–1151, Nov. 1998, doi: 10.1109/63.728341.

[9] N. P. Filho, J. O. P. Pinto, L. E. Borges da Silva, and B. K. Bose, "A simple and ultra-fast DSP-based space vector PWM algorithm and its implementation on a two-level inverter covering undermodulation and overmodulation," in *Proc. 30th Annu. Conf. IEEE Ind. Electron. Soc. (IECON)*, vol. 2, Nov. 2004, pp. 1224–1229, doi: 10.1109/IECON.2004.1431750.

[10] Z. Li, Y. Guo, K. Huang, and X. Zhang, "Synchronized SVPWM algorithm based on superposition principle for the overmodulation region at low switching frequency," in *Proc. 19th Int. Conf. Elect. Mach. Syst. (ICEMS)*, Nov. 2016, pp. 1–6.

[11] A. M. Khambadkone and J. Holtz, "Compensated synchronous PI current controller in overmodulation range and six-step operation of space-vector-modulation-based vector-controlled drives," *IEEE Trans. Ind. Electron.*, vol. 49, no. 3, pp. 574–580, Jun. 2002, doi: 10.1109/TIE.2002.1005382.

[12] A. M. Khambadkone and J. Holtz, "Current control in overmodulation range for space vector modulation based vector controlled induction motor drives," in *Proc. 26th Annu. Conf. IEEE Ind. Electron. Soc. IEEE Int. Conf. Ind. Electron., Control Instrum. 21st Century Technol. Ind. Opportunities (IECON)*, Oct. 2000, pp. 1334–1339, doi: 10.1109/IECON.2000.972315.

[13] S. Venugopal and G. Narayanan, "An overmodulation scheme for vector controlled induction motor drives," in *Proc. Int. Conf. Power Electron., Drives Energy Syst.*, Dec. 2006, pp. 1–6, doi: 10.1109/PEDES.2006.344382.

[14] J. Holtz, "Advanced PWM and predictive control—An overview," *IEEE Trans. Ind. Electron.*, vol. 63, no. 6, pp. 3837–3844, Jun. 2016, doi: 10.1109/TIE.2015.2504347.

[15] C. Piao and J. Y. Hung, "A novel SVPWM overmodulation technique for three-level NPC VSI," in *Proc. IEEE Transp. Electrific. Conf. Expo (ITEC)*, Jun. 2015, pp. 1–6, doi: 10.1109/ITEC.2015.7165744.

[16] S. Li, W. Chen, Y. Yan, T. Shi, and C. Xia, "A multimode space vector overmodulation strategy for ultrasparse matrix converter with improved fundamental voltage transfer ratio," *IEEE Trans. Power Electron.*, vol. 33, no. 8, pp. 6782–6793, Aug. 2018, doi: 10.1109/TPEL.2017.2752748.

[17] J. Chen, R. Ni, T. Li, R. Qiu, and Z. Liu, "The harmonic characteristic of the advanced synchronous SVPWM overmodulation strategy," *IEEE Access*, vol. 7, pp. 148934–148949, 2019, doi: 10.1109/ACCESS.2019.2946654.

[18] Y. Zhu, W. Gu, K. Lu, and Z. Wu, "Vector control of asymmetric dual three-phase PMSM in full modulation range," *IEEE Access*, vol. 8, pp. 104479–104493, 2020, doi: 10.1109/ACCESS.2020.2999647.

[19] F. Bu, T. Pu, Q. Liu, B. Ma, M. Degano, and C. Gerada, "Four-degree-of-freedom overmodulation strategy for five-phase space vector pulsewidth modulation," *IEEE J. Emerg. Sel. Topics Power Electron.*, vol. 9, no. 2, pp. 1578–1590, Apr. 2021, doi: 10.1109/JESTPE.2020.2992659.

[20] J.-H. Park, W. Jo, E.-T. Jeon, S.-H. Kim, C.-H. Lee, J.-H. Lee, J.-H. Lee, J. Yi, and C.-Y. Won, "Variable switching frequency control-based six-step operation method of a traction inverter for driving an interior permanent magnet synchronous motor for a railroad car," *IEEE Access*, vol. 10, pp. 33829–33843, 2022, doi: 10.1109/ACCESS.2022.3162877.

GOKHAN ALTINTAS (Member, IEEE) received the B.S. degree in electrical engineering, control and automation engineering and the M.S. degree in electrical engineering from Istanbul Technical University, Ayazaga Campus, Turkey, in 2015 and 2017, respectively. He is currently pursuing the Ph.D. degree with Istanbul Technical University, Istanbul, Turkey. His research interests include control system design, control of power electronics systems, motor drives, and digital control. Furthermore, he is a member of IEEE Control Systems Society.

DERYA AHMET KOCABAS (Member, IEEE) received the B.S. degree in electrical engineering from ITU, Istanbul, Turkey, in 1994, and the M.Sc. and Ph.D. degrees in electrical engineering program from the Institute of Science and Technology, ITU, in 1997 and 2004, respectively. His main subjects of concern are the design and control of electrical machines, space harmonics, drive systems, and power electronics. In 1995, he joined the Department of Electrical Engineering, Faculty of Electrics and Electronics, ITU, and worked as an Assistant Professor, from 2009 to 2021. He has been working as an Associate Professor, since 2021.